Journal of Power Sources 434 (2019) 226755

Contents lists available at ScienceDirect

Journal of Power Sources

journal homepage: www.elsevier.com/locate/jpowsour

Long-term contamination effect of iron ions on cell performance degradation of proton exchange membrane water electrolyser

Na Li *, Samuel Simon Araya, Søren Knudsen Kær

Aalborg University, Department of Energy Technology, Pontoppidanstræde 111, 9220, Aalborg Øst, Denmark

HIGHLIGHTS

- Long-term Fe^{3+} contamination effect on the single cell performance was studied.
- The cell performance degrade severely with 1 ppm Fe^{3+} contamination.
- Post-mortem analysis of membrane degradation mechanism was carried out.
- Significant membrane thinning and catalyst layers degradation are observed.

GRAPHICAL ABSTRACT

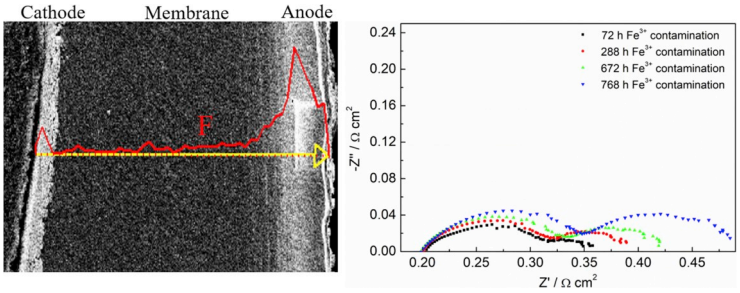

ARTICLE INFO

Keywords:
PEM water electrolysis
Fe^{3+} contamination
Long-term operation
MEA degradation mechanism
Fluoride emission

ABSTRACT

It is known that impurities, especially metal ions in feed water, can cause significant performance degradation of proton exchange membrane water electrolyser (PEM WE). In this study, the long-term effect of iron ion contamination on single cell performance is investigated by introducing $Fe_2(SO_4)_3$ into deionized water fed in PEM WE. Electrochemical impedance spectroscopy (EIS) and polarization curve results were recorded during the test. Results show that with 1 parts per million (ppm, molar ratio) Fe^{3+} contamination at the test condition of 0.5 A/cm^2 and 60 °C, the cell performance degrades severely, especially the charge and mass transfer resistances increase significantly with time. Resistance values obtained through fitting the experiment data with equivalent circuit model were used to better describe the results. The results of Scanning Electron Microscope (SEM) and Energy Dispersive X-ray Spectroscopy (EDX) test illustrate that the existence of Fe^{3+} promote the Fenton reaction, leading to the production of chemical radicals, which degrade the membrane and anode catalyst layer severely.

1. Introduction

Due to the anthropogenic emissions and the consequent environmental issues, decarbonization of the economy and sustainable energy development are hot topics among the experts and scholars. As an efficient and carbon neutral energy vector, hydrogen is considered one of the promising solution to tackle the global energy and environmental crisis [1–3]. However, most of the global hydrogen demand (about 96%) is obtained mainly by steam methane reforming or gasification, only 4% is generated by water electrolysis [4]. Compared with other electrolysers, relevant technological advantages of high efficiency, quick response, high dynamics, high H_2 purity and production capacity, and

* Corresponding author.
E-mail addresses: nal@et.aau.dk (N. Li), ssa@et.aau.dk (S.S. Araya), skk@et.aau.dk (S.K. Kær).

https://doi.org/10.1016/j.jpowsour.2019.226755
Received 4 April 2019; Received in revised form 17 May 2019; Accepted 11 June 2019
Available online 18 June 2019
0378-7753/

more compact design make PEM WE a promising technology for utilizing fluctuating renewable energies to produce hydrogen, while also providing grid balancing services [5–7].

Many researches on PEM WE have been done to promote its commercialization. To meet the targets of capital cost and durability, advanced catalysts with high activity and stability for hydrogen and oxygen evolution have been reported [3,8,9]. However, while durability studies of PEM WE are important, the literature is still limited.

The durability of PEM WE is primarily associated with the chemical stability of the membrane electrode assembly (MEA). According to many experimental and model results, the operating parameters such as current density [5,10–15], temperature [11–13], pressure [16–18], etc., may have strong effect on MEA durability during the operating process. Another factor that should not be ignored during the PEM WE operating process is the external feed water impurity, which is often mentioned but seldom fully investigated in many researches. In water electrolysis systems, the quality of the circulating water may get worse after long time operation, though a water purification system is employed, due to the existence of metallic impurities such as Fe^{3+}, Al^{3+} Cu^{2+}, Ca^{2+}, Ni^{2+}, Na^{+}, etc. These impurities in the circulating water can be originated from many sources, such as the fabricating process of MEA, components' corrosion, electrocatalysts' dissolution and so on [6,19–21]. There have been some articles which studied the effect of circulating water quantity [22] and flow rate [23] on performance of PEM WE. However, researches about the influence of feed water purity on MEA degradation mechanism analysis are scarce. According to some research results from proton exchange membrane fuel cell (PEMFC), trace amount of cationic contaminants originated from feed water are responsible for severe cell performance degradation [24–26].

These studies found that multivalent cation ions such as Al^{3+}, Fe^{3+}, Cr^{3+}, Ni^{2+}, Mg^{2+} in feed water have stronger affinity for sulfonic acid groups in Nafion than protons and could easily substitute protons in the ion exchange process, leading to increased ohmic resistance and reduced ion conductivity [27–30]. Qi et al. [28] investigated the influence of Al^{3+} on PEMFC performance and found that Al^{3+} could occupy the acid site in the membrane and decrease cell performance. Li et al. [25] studied the contamination effect of Al^{3+} and Fe^{3+}, and showed that 5 ppm Fe^{3+} could cause a sudden cell failure, and Al^{3+} could reduce the kinetics and electron transfer number. The contamination effects of many other cations, such as Ca^{2+} [27,29,31], Na^{+} [20,27], Cu^{2+} [32], Fe^{2+} and Ni^{+} [6,33], etc., were also investigated on PEMFC.

Drawing on the research experience of fuel cells, a few works of cation ions contamination short time effect on PEM WE have been carried out. Zhang et al. [34,35] found that anode Na^{+} poisoning degrades the cell performance more severely than cathode, and the severity and poisoning rate depended on the Na^{+} concentration [34,35]. Wang et al. [19] studied the ferric ion contamination of solid polymer electrolyte water electrolysis, and the results showed that Fe^{3+} ions degraded the cell performance greatly. As a commonly seen metal ion in the feed water, the degradation mechanism analysis of Fe^{3+} impurity contamination deserves more attention. In this study, long-term Fe^{3+} ion contamination effects on the performance of single PEM WE cell were investigated, and the degradation mechanism are discussed.

2. Methodology

2.1. Single cell experimental set-up

The membrane used in the experiment has an active area of 2.89 cm^2 (1.7 cm × 1.7 cm). The membrane electrode assembly (MEA) consists of 0.3 mg cm^{-2} of IrO_2, Nafion117, 0.5 mg cm^{-2} of Pt/C, and a carbon cloth (Sigracet 35 DC) from anode side to cathode side, which serve as anode catalyst, solid electrolyte, cathode catalyst and cathode porous transport layer, respectively. A 350 mm thick Ti felt of 81% porosity and fiber diameter of 20 mm was employed as the anode porous transport layer. The MEA was sandwiched with the end plates and current collectors on both sides, and screws and nuts were used to fix the cell assembly.

2.2. Test set-up and procedures

The test bench used in these tests is a single cell set-up of two-electrodes. As can be seen in Fig. 1, the anode side of the cell, which works as the working electrode, is connected with a water recirculation system. A toroidal shell heater is employed to heat the feed water, which was then fed to the cell to keep it at constant temperature. The feed water circulates between the cell and the water tank through a pump. The produced O_2 exits the cell through the anode side together with circulating water and H_2 exits through the cathode side of the cell to the fume hood.

A Gamry Reference 3000 potentiostat/galvanostat is connected to the cell and works as the power supply. The single cell was operated galvanostatically at 0.5 A cm^{-2} and the temperature was kept constant at 60 °C. The flow rate of feed water was 270 mL min^{-1}, which is high enough over-stoichiometry both feeding the reaction and for cooling. The compression pressure was set to 2.61 MPa by controlling the length of the springs on the screws. Before the tests, the cell was run for 72 h with deionized (DI) water as a break-in step.

For the contamination tests, a solution containing 1 ppm Fe^{3+} was prepared by diluting a 70 mL prefabricated $Fe_2(SO_4)_3$ solution containing 10 ppm Fe^{3+} ions with 700 mL deionized (DI) water. The pH of the contaminated solution was kept to 2 in order to prevent the hydrolysis of Fe^{3+}. The contamination test lasted for 829 h.

The water recirculation system is connected with the anode side of the single cell through non-metallic pipes, which will neither be corroded by the contaminated solution nor contribute with more cationic contaminants. Besides, recirculating the water is advantageous, because other than being economic and similar to real systems, it is also more practical for such long-term experiments, as it avoids the need for changing the solution frequently or preparing a big reservoir of solution.

2.3. Characterizations

A Gamry Reference 3000 potentiostat/galvanostat and booster were used to carry out the electrochemical impedance spectroscopy (EIS) and polarization measurements. The frequency range for EIS measurements was from 60000 Hz to 0.01 Hz and 10 measurement points per decade were recorded for each EIS sweep. The polarization curves were measured in a potentiostatic mode from 1 V to 2.5 V.

After the electrochemical measurements, the cell was disassembled and a post-mortem analysis of the MEA was carried out through Scanning Electron Microscopy (SEM) and Energy Dispersive X-ray Spectroscopy (EDX). The cross-sections of MEAs of both fresh sample and contaminated sample were prepared by cutting into smaller pieces with a sharp knife and then placed on the sample stage for tests. The thickness of the different layers were measured and then line scans of different elements were collected to observe the elemental distribution.

3. Results and discussion

3.1. Voltage change and degradation rate

The effect of 1 ppm Fe^{3+} ion contamination on cell overall performance is investigated through a constant current operation in this study. As can be seen in Fig. 2, before the Fe^{3+} was introduced, the cell voltage degradation rate was 5.2 μV h^{-1}. However the cell voltage increased from 1.637 V to 1.657 V immediately after introducing Fe^{3+} ions into the DI water feed, and kept increasing sharply in the presence of Fe^{3+}. After about 432 h operation, the cell experienced an unexpected sudden stop and upon restart the voltage decreased, but then continued to degrade at similar rate. The sudden cell voltage decrease due to the unexpected stop can be attribute to the fact that oxygen produced during

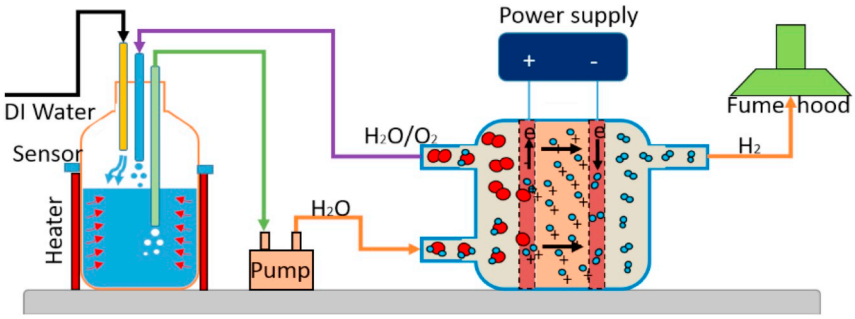

Fig. 1. Schematic of the test bench.

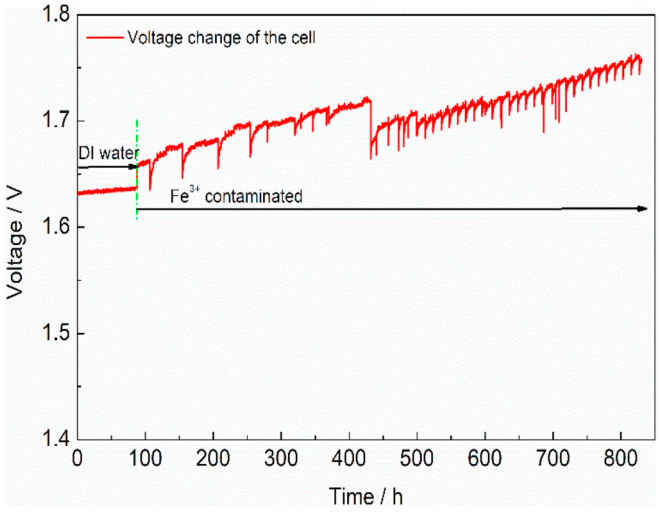

Fig. 2. Voltage change throughout the entire test period.

the constant load operation may be trapped in the flow channels, and this unexpected stop can give time for the trapped oxygen to escape from the channels, which could reduce the mass transfer resistance, and thus increase the cell performance [18].

The immediate voltage increase after introducing Fe^{3+} ions into the feed water indicates that the contamination of Fe^{3+} ions degrades the cell performance greatly even with a very low concentration of 1 ppm. An interesting finding is that the cell voltage decreased a little bit after each EIS measurement, which could be due to the fact that the sinusoidal signal gives a current cycling effect, which may have a reconditioning effect.

Moreover, though the Fe^{3+} ion concentration in the circulating solution reduces with time because of the adsorption or accumulation on the membrane and catalyst layers and the exhaust from cathode outlet, the overall trend of cell voltage keeps a sustained growth. This is reasonable because the adsorption on the membrane continues and is cumulative. The average cell voltage degradation rate from when introducing Fe^{3+} ions to the end of the test is calculated to be 128.9 $\mu V\,h^{-1}$. Compared with the acceptable degradation rate of 2–10 $\mu V\,h^{-1}$ [6,36], this degradation rate with of Fe^{3+} in the feed water is deemed quite high.

3.2. Polarization curve analysis

Fig. 3 shows the polarization curves obtained at different time point during the tests. It can be seen that the cell voltage increased with time after Fe^{3+} ions were introduced into DI water. In the magnification of the initial part of the polarization curves on the left figure in Fig. 3 it can be seen that the slopes of curves at low current density are steeper than those at high current density, especially for the condition of Fe^{3+} contamination. This is reasonable because the evolution kinetics dominate the whole process at low current density. In the presence of Fe^{3+}, the reaction kinetics are slowed because Fe^{3+} ions have higher affinity for SO_3^- group but lower ionic mobilities in Nafion than H^+, where they could occupy ion exchange sites and agglomorate on the catalyst layers with time, and thus, decrease the conductivity of the membrane as well

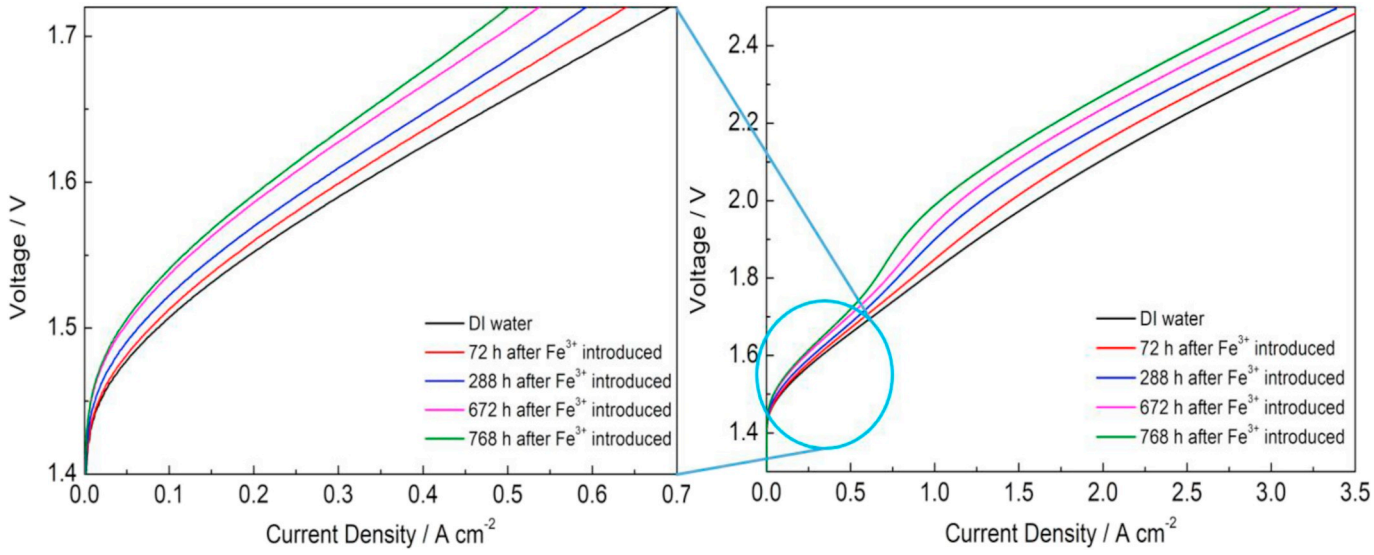

Fig. 3. Polarization curves at different time point.

as the reaction kinetics of both sides [25,27].

In order to analyze the polarization resistance (R_{slop}) more intuitively, the variation trend of the polarization resistances at different time points were obtained by calculating the slopes of IV curves. As can be seen in Fig. 4, the polarizarion resistance increases clearly with time after Fe^{3+} ions were introduced into feed water both at high and low current density. With increase in current density, the values of R_{slop} decreased dramatically, which could be due enhanced reaction kinetics of both anode and cathode side, which contribute to a better cell performance, which can also be seen in Fig. 3.

3.3. EIS test analysis

EIS measurements were carried out to further investigate the performance degradation of the single cell. The equivalent circuit shown in Fig. 5 was used to simulate the EIS data in Fig. 6. R_L is inductive resistance, associated with the inductance of cables and other components in the system [18,22,37]. R_{ohm} represents the ohmic resistance of the cell, consisting of ionic resistance, contact resistance and all metallic components resistance, which equals to the high frequency intercept on the real axis (left) in Fig. 5. Considering the high over-stoichiometric water flow rate, the mass transfer resistance in this study is minimized. Therefor R_1 in the equivalent circuit, which is in parallel with a constant phase element (CPE1), represents the resistance which is usually dominated by the anode charge transfer processes, and equals to the arc diameter of the first semi-circles of EIS spectra in Fig. 5. R_2, in parallel with CPE2 in the equivalent circuit, represents mainly the resistance of cathode charge transfer process, and corresponds to the arc diameter of the second semi-circles of EIS spectra in Fig. 5. Taking into account the surface roughness factor and the non-uniformly distributed double layer capacitance of electrolyzer, the constant phase elements (CPEs) were employed to substitute the double layer capacitance in the equivalent circuit to decrease the deviation [38–40]. The obtained resistance values are shown in Table 1.

It is well known that the cathode side charge transfer resistance in the evolution reaction is rather small compared with the anode side charge transfer resistance because of the quite fast reaction rate of hydrogen evolution on the cathode [41]. As shown in Fig. 6 (a), at the begainning of the test, the R_1 values for both DI water test and short time contamination test are all much bigger than the values of R_2, about fivefold from the values in Table 1. The values of R_{ohm} and R_1 of the single cell immediately after introducing Fe^{3+} ions are almost the same as those under DI water condition, but the R_2 values increase markedly, which can also be seen in Table 1. This indicates that the Fe^{3+} contamination affects the hydrogen evolution reaction firstly, which maybe due to the iron ions adsorbed on the membrane, affecting proton transportation and thus lowering the kinetics of hydrogen evolution reaction. After 24 h operation with Fe^{3+} contamination, both the R_1 and R_2 value begin to increase. It can also be seen in Fig. 6 (b) and Table 1 that the values of R_1 and R_2 increase significantly with time under the condition of Fe^{3+} contamination. R_1 value under the condition of DI water is 0.105 Ω, and reached to 0.165 Ω at the end of the test, with an increase of 50 mΩ, while the value of R_2 increased by 115 mΩ from 0.022 Ω to 0.137 Ω. However, the ohmic resistance of the cell doesn't show big changes, where it slightly increases for the first 72 h and then decreases slightly with time, which maybe owning to the membrane thinning under the Fe^{3+} contamination. These results indicate that the charge transfer processes of both anode and cathode side are severely affected by Fe^{3+} ions, especially the cathode side, which is in line with the results obtained from the polarization curves in section 3.2.

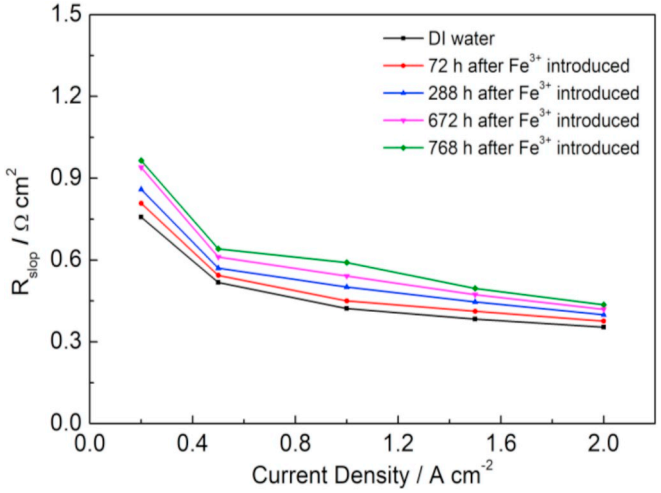

Fig. 4. Polarization resistances from IV curves at different current density.

3.4. SEM images and EDX results analysis

To futher understand the degradation mechanism of iron ion contamination, SEM and EDX tests were carried out on the cross-section of both new and contaminated MEAs. Fig. 7 shows the SEM images of MEAs of both (a) new sample and (b) contaminated sample. For new MEA in Fig. 7 (a), the thicknesses of anode catalyst layer, membrane and cathode catalyst layer are 19.44 μm, 157.3 μm, and 8.043 μm, respectively. However, for Fe^{3+} contaminated MEA in Fig. 7 (b), the thicknesses of cathode catalyst layer and membrane are 11.11 μm and 150.2 μm, respectively, while the thickness of the anode catalyst layer reduces to around 30% of original thickness. Moreover, a membrane thinning can be seen on the contaminated MEA, where the thickness decreased by 7.1 μm compared with the new MEA, which can explain the slight decrease in ohmic resistance with time. However, while the cathode catalyst layer of contaminated sample became a little thicker, the anode catalyst layer became dramatically thinner, which can partly be explained by the higher tolerance of the cathode materials in the presence of Fe^{3+} contamination compared to anode [19]. The Fe^{3+} has higher affinity for $–SO^{3-}$ group and can replace protons during the ion exchange process, and this can lead to an increase in charge transfer resistance [6,19,27]. This hinders the protons conduction to the cathode, which may lead to a competing H_2 production reaction, $2H_2O + 2e^- \rightarrow H_2 + 2OH^-$, on the anode catalyst layer [34]. H_2 on the oxygen side can lead to hydrogen peroxide formation, which in turn can cause catalyst disolution due to radicals formation, which is reported to be catalysed by Fe ions [42]. All these factors can contribute to more severe anode catalyst degradation than that of cathode.

It is generally known that the Nafion membrane degradation can be predicted by the flouride release [20], and hence, the fluorine elemental distribution on the cross-section of the MEAs can also reflect the degradation of the Nafion membrane. Fig. 8 shows the SEM images of the cross-section of the same fresh and contaminated MEAs in Fig. 7, along with the elemental distribution obtained from the EDX line scanning, which was employed to demonstrate the elemental analysis of the membrane. As can be seen from Fig. 8 (a), the flourine is evenly distributed on the membrane of the fresh MEA with a high content. However after contamination test, the flourine distribution on the membrane was greatly changed. As shown in Fig. 8 (b) the content of fluorine on the membrane near the cathode side decreased significantly, which indicates that a large amount of flourine were released from the membrane near the cathode side. This result is consistent with the literature, where it is reported that the membrane degradation mostly occurred on the cathode side [12,42]. During the operation, the oxygen produced at anode can crossover to the cathode side through the membrane, and reacte with protons to produce hydrogen peroxide (H_2O_2) through a two electrons O_2 reduction reaction. H_2O_2 could then decompose to hydroxyl radicals that are known to attack the membrane in the presence of Fe^{3+}, since Fe^{3+} ions promote the hydroxyl radicals formation through a modified Fenton reaction [20,25], as follows:

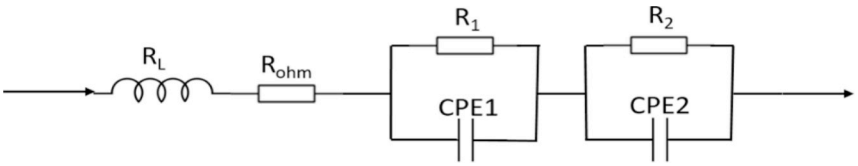

Fig. 5. Equivalent circuit for impedance data fitting.

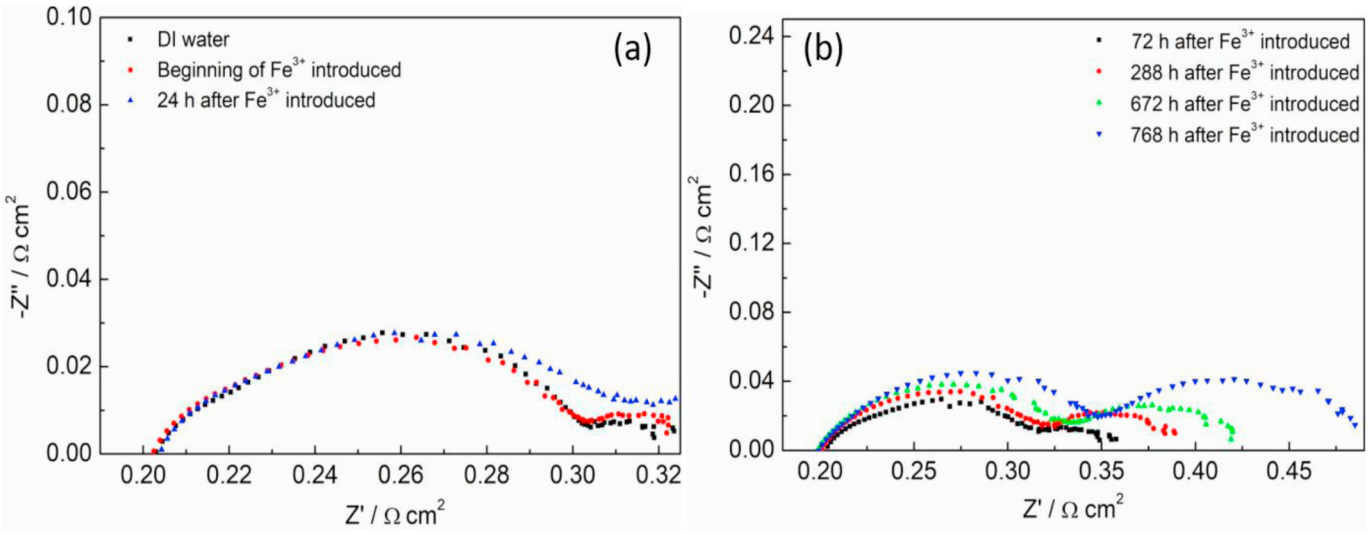

Fig. 6. Electrochemical Impedance Spectra at different test points.

Table 1
Impedance values obtained by fitting the experiment data to the equivalent circuit.

Test condition	R_{ohm}/Ω cm^2	R_1/Ω cm^2	R_2/Ω cm^2
DI water	0.203	0.105	0.022
After 1 ppm Fe^{3+} introduced immediately	0.202	0.106	0.027
24 h after 1 ppm Fe^{3+} introduced	0.204	0.111	0.043
72 h after 1 ppm Fe^{3+} introduced	0.204	0.117	0.041
288 h after 1 ppm Fe^{3+} introduced	0.201	0.129	0.068
672 h after 1 ppm Fe^{3+} introduced	0.199	0.147	0.086
768 h after 1 ppm Fe^{3+} introduced	0.201	0.165	0.137

$$\text{Nafion - } Fe^{3+} + H_2O_2 \rightarrow \text{Nafion - } Fe^{2+} + HO_2^{\cdot} + H^+ \quad (1)$$

$$\text{Nafion - } Fe^{2+} + H_2O_2 \rightarrow \text{Nafion - } Fe^{3+} + HO^{\cdot} + OH^- \quad (2)$$

The Fe distribution in Fig. 8 (c) futher support this phenomenon. As can be seen in Fig. 8 (c), the amount of Fe on the cathode side is higher than that on the membrane and anode side, which illustrates that the iron ions transferred from anode side through the membrane to the cathode side and accumulated on the cathode side, where they facilitate for the Fenton reaction. Besides, Fe^{3+} has a Nernst potentials of −0.01 V vs. SHE, which contribute to the underpotential deposition on the

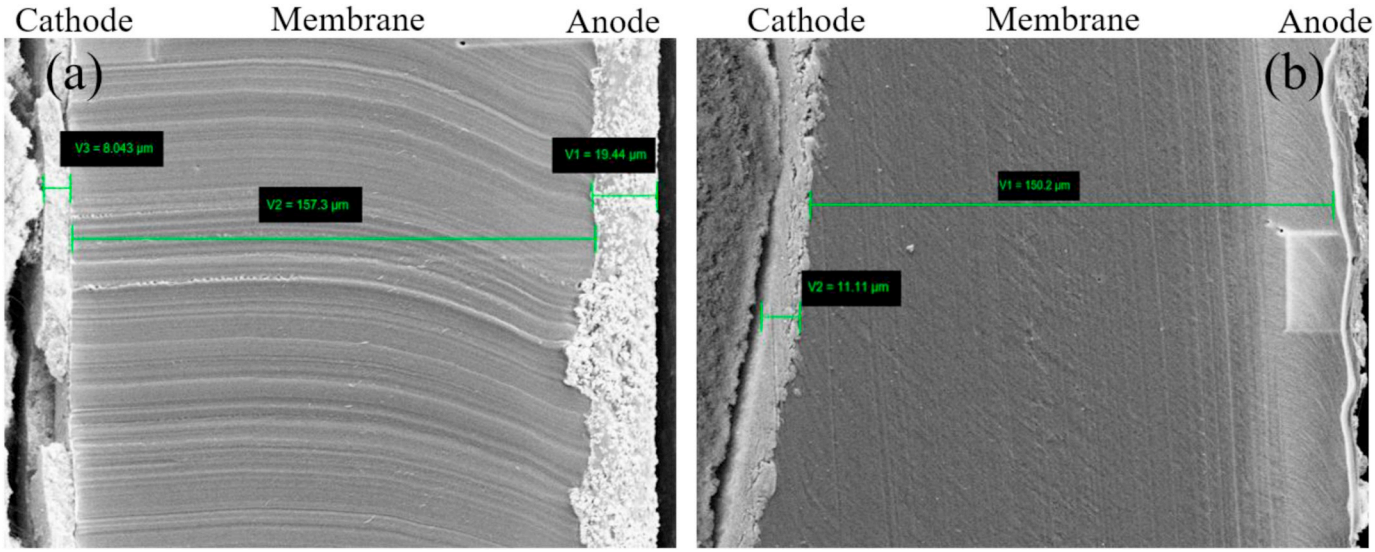

Fig. 7. SEM images of (a) new sample and (b) contaminated sample.

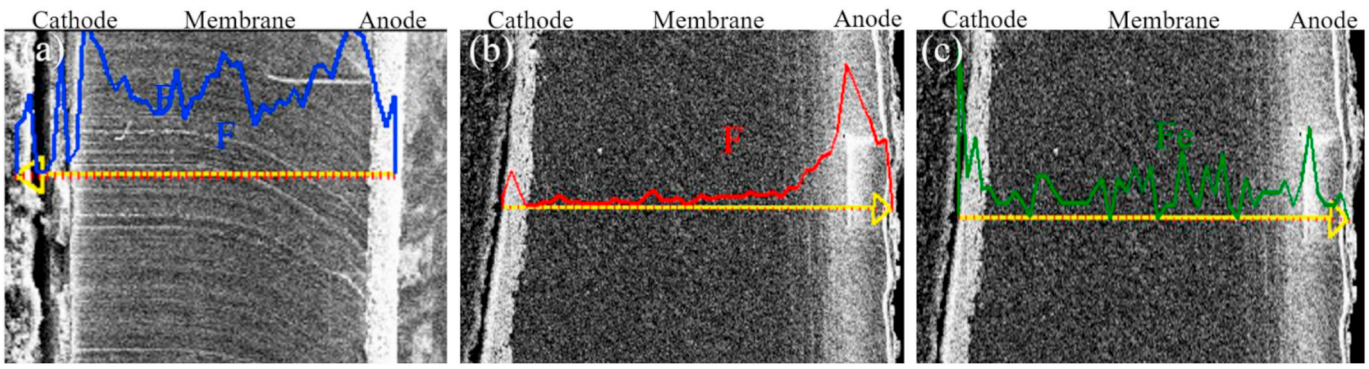

Fig. 8. Line scanning EDX images about the distribution of F (a) fresh and (b) the contaminated MEA of the cross-section and (c) the Fe distribution at the cross-section of the contaminated MEA.

cathode site [43]. These will all degrade the cell performance significantly. The accumulation of the Fe^{3+} ions on the cathode side will reduce the ionic conductivity of the membrane and lead to increased ionic resistance, resulting in increased ohmic resistance which is counteracted by the membrane thinning. Besides, the reduced number of protons reaching the cathode electrode lead to reduced rate of hydrogen production at the cathode, which in turn will cause increased partial pressure on the anode side and thus promote oxygen crossover phenomenon. Also, the accumulation of Fe^{3+} ions on the cathode side will reduce the active catalyst sites, leading to sluggish hydrogen reaction kinetics and increased electrochemical overpotential, which can explain the great increase in charge transfer resistance on the cathode side. Furthermore, the hindered hydrogen ions will combine with oxygen to form hydrogen peroxide, which is most likely to produce chemical radicals in the presence of Fe^{3+} ions that attack the membrane and poison the catalyst [19,42,44].

4. Conclusion

Long duration (829 h) contamination effect of 1 ppm Fe^{3+} on single cell performance degradation was studied by introducing Fe^{3+} into the feed water. Significant performance decrease was observed, the degradation rate reaches to 128.9 $\mu V\,h^{-1}$ after 829 h contamination test. Polarization and EIS measurements depict that the charge transfer resistance, especially on the cathode side increased significantly with time after the introduction of 1 ppm Fe^{3+}, which is due to the iron ions occupying the ion exchange sites on the membrane and active catalytic sites on the catalyst layer. The SEM and EDX test showed that Fe^{3+} ions transferred through the membrane from anode to cathode and accumulated on the cathode side. The membrane is believed to have been attacked by radicals formed from hydrogen peroxide in the presence of Fe^{3+}, as manifested by the reduced fluoride count on the cathode side of the contaminated MEA and a 7.1 μm membrane thickness reduce. Although the effects are not directly measurable, the dissolution of the anode catalyst layer observed by the significant thinning of the anode in the SEM images may have contributed to the overall cell performance degradation and could be crucial for the stability and durability of the cell.

Acknowledgments

The authors would like to acknowledge the financial support from Innovation Fund Denmark through the e-STORE project, Grant No. 4106-00025B. Na Li appreciates China Scholarship Council for the financial support.

References

[1] S.M.M. Ehteshami, S.H. Chan, The role of hydrogen and fuel cells to store renewable energy in the future energy network – potentials and challenges, Energy Policy 73 (2014) 103–109, https://doi.org/10.1016/j.enpol.2014.04.046.
[2] F. Barbir, PEM electrolysis for production of hydrogen from renewable energy sources, Sol. Energy 78 (2005) 661–669, https://doi.org/10.1016/j.solener.2004.09.003.
[3] K. Liu, H. Zhong, F. Meng, X. Zhang, J. Yan, Q. Jiang, Recent advances in metal–nitrogen–carbon catalysts for electrochemical water splitting, Mater. Chem. Front. 1 (2017) 2155–2173, https://doi.org/10.1039/c7qm00119c.
[4] A.C. Luca Bertuccioli, David Hart, Franz Lehner, Ben Madden, Eleanor Standen, Development of Water Electrolysis in the European Union, FCH-JU Report, 2014.
[5] C. Rakousky, G.P. Keeley, K. Wippermann, M. Carmo, D. Stolten, The stability challenge on the pathway to high-current-density polymer electrolyte membrane water electrolyzers, Electrochim. Acta 278 (2018) 324–331, https://doi.org/10.1016/j.electacta.2018.04.154.
[6] S. Sun, Z. Shao, H. Yu, G. Li, B. Yi, Investigations on degradation of the long-term proton exchange membrane water electrolysis stack, J. Power Sources 267 (2014) 515–520, https://doi.org/10.1016/j.jpowsour.2014.05.117.
[7] A. Marshall, B. Børresen, G. Hagen, M. Tsypkin, R. Tunold, Hydrogen production by advanced proton exchange membrane (PEM) water electrolysers—reduced energy consumption by improved electrocatalysis, Energy 32 (2007) 431–436, https://doi.org/10.1016/j.energy.2006.07.014.
[8] K.H. Liu, H.X. Zhong, S.J. Li, Y.X. Duan, M.M. Shi, X.B. Zhang, J.M. Yan, Q. Jiang, Advanced catalysts for sustainable hydrogen generation and storage via hydrogen evolution and carbon dioxide/nitrogen reduction reactions, Prog. Mater. Sci. 92 (2018) 64–111, https://doi.org/10.1016/j.pmatsci.2017.09.001.
[9] J. Wang, H.X. Zhong, Z.L. Wang, F.L. Meng, X.B. Zhang, Integrated three-dimensional carbon paper/carbon tubes/cobalt-sulfide sheets as an efficient electrode for overall water splitting, ACS Nano 10 (2016) 2342–2348, https://doi.org/10.1021/acsnano.5b07126.
[10] P. Lettenmeier, R. Wang, R. Abouatallah, S. Helmly, T. Morawietz, R. Hiesgen, S. Kolb, F. Burggraf, J. Kallo, A.S. Gago, K.A. Friedrich, Durable membrane electrode assemblies for proton exchange membrane electrolyzer systems operating at high current densities, Electrochim. Acta 210 (2016) 502–511, https://doi.org/10.1016/j.electacta.2016.04.164.
[11] M. Chandesris, V. Médeau, N. Guillet, S. Chelghoum, D. Thoby, F. Fouda-Onana, Membrane degradation in PEM water electrolyzer: numerical modeling and experimental evidence of the influence of temperature and current density, Int. J. Hydrogen Energy 40 (2015) 1353–1366, https://doi.org/10.1016/j.ijhydene.2014.11.111.
[12] F. Fouda-Onana, M. Chandesris, V. Médeau, S. Chelghoum, D. Thoby, N. Guillet, Investigation on the degradation of MEAs for PEM water electrolysers part I: effects of testing conditions on MEA performances and membrane properties, Int. J. Hydrogen Energy 41 (2016) 16627–16636, https://doi.org/10.1016/j.ijhydene.2016.07.125.
[13] C. Immerz, M. Schweins, P. Trinke, B. Bensmann, M. Paidar, T. Bystroň, K. Bouzek, R. Hanke-Rauschenbach, Experimental characterization of inhomogeneity in current density and temperature distribution along a single-channel PEM water electrolysis cell, Electrochim. Acta 260 (2018) 582–588, https://doi.org/10.1016/j.electacta.2017.12.087.
[14] A.S. Gago, J. Bürkle, P. Lettenmeier, T. Morawietz, M. Handl, R. Hiesgen, F. Burggraf, P.A. Valles Beltran, K.A. Friedrich, Degradation of proton exchange membrane (PEM) electrolysis: the influence of current density, ECS Trans. 86 (2018) 695–700, https://doi.org/10.1149/08613.0695ecst.
[15] B.B.P. Trinke, R. Hanke-Rauschenbach, Current density effect on hydrogen permeation in PEM water electrolyzers, Int. J. Hydrogen Energy 42 (2017) 14355–14366, https://doi.org/10.1016/j.ijhydene.2017.03.231.
[16] S.A. Grigoriev, K.A. Dzhus, D.G. Bessarabov, P. Millet, Failure of PEM water electrolysis cells: case study involving anode dissolution and membrane thinning, Int. J. Hydrogen Energy 39 (2014) 20440–20446, https://doi.org/10.1016/j.ijhydene.2014.05.043.

[17] B. Verdin, F. Fouda-Onana, S. Germe, G. Serre, P.A. Jacques, P. Millet, Operando current mapping on PEM water electrolysis cells. Influence of mechanical stress, Int. J. Hydrogen Energy 42 (2017) 25848–25859, https://doi.org/10.1016/j.ijhydene.2017.08.189.
[18] S.H. Frensch, A.C. Olesen, S.S. Araya, S.K. Kær, Model-supported characterization of a PEM water electrolysis cell for the effect of compression, Electrochim. Acta 263 (2018) 228–236, https://doi.org/10.1016/j.electacta.2018.01.040.
[19] X. Wang, L. Zhang, G. Li, G. Zhang, Z.-G. Shao, B. Yi, The influence of Ferric ion contamination on the solid polymer electrolyte water electrolysis performance, Electrochim. Acta 158 (2015) 253–257, https://doi.org/10.1016/j.electacta.2015.01.140.
[20] A. Pozio, R.F. Silva, M. De Francesco, L. Giorgi, Nafion degradation in PEFCs from end plate iron contamination, Electrochim. Acta 48 (2003) 1543–1549, https://doi.org/10.1016/s0013-4686(03)00026-4.
[21] X. Cheng, Z. Shi, N. Glass, L. Zhang, J. Zhang, D. Song, Z.-S. Liu, H. Wang, J. Shen, A review of PEM hydrogen fuel cell contamination: impacts, mechanisms, and mitigation, J. Power Sources 165 (2007) 739–756, https://doi.org/10.1016/j.jpowsour.2006.12.012.
[22] S. Sun, Y. Xiao, D. Liang, Z. Shao, H. Yu, M. Hou, B. Yi, Behaviors of a proton exchange membrane electrolyzer under water starvation, RSC Adv. 5 (2015) 14506–14513, https://doi.org/10.1039/c4ra14104k.
[23] Ö.F. Selamet, F. Becerikli, M.D. Mat, Y. Kaplan, Development and testing of a highly efficient proton exchange membrane (PEM) electrolyzer stack, Int. J. Hydrogen Energy 36 (2011) 11480–11487, https://doi.org/10.1016/j.ijhydene.2011.01.129.
[24] M.A. Uddin, J. Qi, X. Wang, U. Pasaogullari, L. Bonville, Distributed cation contamination from cathode to anode direction in polymer electrolyte fuel cells, Int. J. Hydrogen Energy 40 (2015) 13099–13105, https://doi.org/10.1016/j.ijhydene.2015.07.134.
[25] H. Li, K. Tsay, H. Wang, J. Shen, S. Wu, J. Zhang, N. Jia, S. Wessel, R. Abouatallah, N. Joos, Durability of PEM fuel cell cathode in the presence of Fe^{3+} and Al^{3+}, J. Power Sources 195 (2010) 8089–8093, https://doi.org/10.1016/j.jpowsour.2010.07.003.
[26] J. Wu, X.Z. Yuan, J.J. Martin, H. Wang, J. Zhang, J. Shen, S. Wu, W. Merida, A review of PEM fuel cell durability: degradation mechanisms and mitigation strategies, J. Power Sources 184 (2008) 104–119, https://doi.org/10.1016/j.jpowsour.2008.06.006.
[27] K. Hongsirikarn, J.G. Goodwin, S. Greenway, S. Creager, Effect of cations (Na^{+}, Ca^{2+}, Fe^{3+}) on the conductivity of a Nafion membrane, J. Power Sources 195 (2010) 7213–7220, https://doi.org/10.1016/j.jpowsour.2010.05.005.
[28] J. Qi, X.F. Wang, U. Pasaogullari, L. Bonville, T. Molter, Effect of Al^{3+} contaminant on polymer electrolyte fuel cell performance, J. Electrochem. Soc. 160 (2013) F916–F922, https://doi.org/10.1149/2.022309jes.
[29] C.J. Banas, M.A. Uddin, J. Park, L.J. Bonville, U. Pasaogullari, Thinning of cathode catalyst layer in polymer electrolyte fuel cells due to foreign cation contamination, J. Electrochem. Soc. 165 (2018) F3015–F3023, https://doi.org/10.1149/2.0021806jes.
[30] M.A. Uddin, X.F. Wang, J. Qi, M.O. Ozdemir, U. Pasaogullari, L. Bonville, T. Molter, Effect of chloride on PEFCs in presence of various cations, J. Electrochem. Soc. 162 (2015) F373–F379, https://doi.org/10.1149/2.0291504jes.
[31] M.A. Uddin, X. Wang, J. Park, U. Pasaogullari, L. Bonville, Distributed effects of calcium ion contaminant on polymer electrolyte fuel cell performance, J. Power Sources 296 (2015) 64–69, https://doi.org/10.1016/j.jpowsour.2015.07.020.
[32] T. Okada, Y. Ayato, M. Yuasa, I. Sekine, The effect of impurity cations on the transport characteristics of perfluorosulfonated ionomer membranes, J. Phys. Chem. B 103 (1999) 3315–3322, https://doi.org/10.1021/jp983762d.
[33] M.J. Kelly, G. Fafilek, J.O. Besenhard, H. Kronberger, G.E. Nauer, Contaminant absorption and conductivity in polymer electrolyte membranes, J. Power Sources 145 (2005) 249–252, https://doi.org/10.1016/j.jpowsour.2005.01.064.
[34] L. Zhang, X. Jie, Z.-G. Shao, X. Wang, B. Yi, The dynamic-state effects of sodium ion contamination on the solid polymer electrolyte water electrolysis, J. Power Sources 241 (2013) 341–348, https://doi.org/10.1016/j.jpowsour.2013.04.049.
[35] L. Zhang, X. Jie, Z.-G. Shao, Z.-M. Zhou, G. Xiao, B. Yi, The influence of sodium ion on the solid polymer electrolyte water electrolysis, Int. J. Hydrogen Energy 37 (2012) 1321–1325, https://doi.org/10.1016/j.ijhydene.2011.10.023.
[36] Q. Feng, X.Z. Yuan, G. Liu, B. Wei, Z. Zhang, H. Li, H. Wang, A review of proton exchange membrane water electrolysis on degradation mechanisms and mitigation strategies, J. Power Sources 366 (2017) 33–55, https://doi.org/10.1016/j.jpowsour.2017.09.006.
[37] X. Yuan, H. Wang, J. Colinsun, J. Zhang, AC impedance technique in PEM fuel cell diagnosis—a review, Int. J. Hydrogen Energy 32 (2007) 4365–4380, https://doi.org/10.1016/j.ijhydene.2007.05.036.
[38] M.E. Orazem, N. Pébère, B. Tribollet, Enhanced graphical representation of electrochemical impedance data, J. Electrochem. Soc. 153 (2006) B129, https://doi.org/10.1149/1.2168377.
[39] P. Córdoba-Torres, T.J. Mesquita, O. Devos, B. Tribollet, V. Roche, R.P. Nogueira, On the intrinsic coupling between constant-phase element parameters α and Q in electrochemical impedance spectroscopy, Electrochim. Acta 72 (2012) 172–178, https://doi.org/10.1016/j.electacta.2012.04.020.
[40] S.T. Stefania Siracusano, Nicola Briguglio, Vincenzo Baglio ID, Antonino S. Aricò, Electrochemical characterization of a PEMEC using impedance spectroscopy, Materials 11 (2018) 1368, https://doi.org/10.1149/2.0651713jes.
[41] I. Dedigama, P. Angeli, K. Ayers, J.B. Robinson, P.R. Shearing, D. Tsaoulidis, D.J.L. Brett, In situ diagnostic techniques for characterisation of polymer electrolyte membrane water electrolysers – flow visualisation and electrochemical impedance spectroscopy, Int. J. Hydrogen Energy 39 (2014) 4468–4482, https://doi.org/10.1016/j.ijhydene.2014.01.026.
[42] S.H. Frensch, G. Serre, F. Fouda-Onana, H.C. Jensen, M.L. Christensen, S.S. Araya, S.K. Kær, Impact of iron and hydrogen peroxide on membrane degradation for polymer electrolyte membrane water electrolysis: computational and experimental investigation on fluoride emission, J. Power Sources 420 (2019) 54–62, https://doi.org/10.1016/j.jpowsour.2019.02.076.
[43] E.R. Kotz, S. Stucki, Ruthenium dioxide as a hydrogen-evolving cathode, J. Appl. Electrochem. 17 (1987) 1190–1197, https://doi.org/10.1007/Bf01023602.
[44] Lorenz Gubler, Sindy M. Dockheer, W.H. Koppenol, Radical ($HO^{\bullet}$, $H^{\bullet}$ and $HOO^{\bullet}$) formation and ionomer degradation in polymer electrolyte fuel cells, J. Electrochem. Soc. 158 (2011) B755–B769, https://doi.org/10.1149/1.3581040.